Journal of Colloid and Interface Science 525 (2018) 161–165

Contents lists available at ScienceDirect

Journal of Colloid and Interface Science

journal homepage: www.elsevier.com/locate/jcis

Regular Article

# Capillary condensation and gelling of microemulsions with clay additives

Manuchar Gvaramia [a,b], Gaetano Mangiapia [a,c], Peter Falus [d], Michael Ohl [e], Olaf Holderer [a], Henrich Frielinghaus [a,*]

[a] Jülich Centre for Neutron Science at MLZ, Forschungszentrum Jülich GmbH, Lichtenbergstrasse 1, 85747 Garching, Germany
[b] Ilia Vekua Sukhumi Institute of Physics and Technologies, 7 Mindeli Str., 0186 Tbilisi, Georgia
[c] Helmholtz-Zentrum Geesthacht GmbH, German Engineering Materials Science Centre at Heinz Maier-Leibnitz Zentrum, Lichenbergstr. 1, 85748 Garching bei München, Germany
[d] Institut Laue Langevin, 71 Avenue des Martyrs, CS 20156, Cedex 9, 38042 Grenoble, France
[e] Jülich Centre for Neutron Sciences JCNS-1, Forschungszentrum Jülich GmbH, Leo Brandt Straße, 52425 Jülich, Germany

## GRAPHICAL ABSTRACT

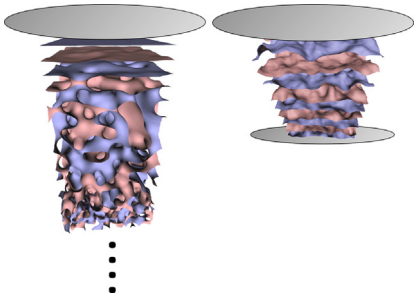

## ARTICLE INFO

*Article history:*
Received 8 March 2018
Revised 6 April 2018
Accepted 6 April 2018
Available online 22 April 2018

*Keywords:*
Microemulsion
Clay
Capillary condensation
Neutron scattering

## ABSTRACT

The capillary condensation in bicontinuous microemulsions takes place when two parallel surfaces are narrowed that result in a completely lamellar microemulsion. We expected that this phase transition is also observable when the amount of hydrophilic surfaces from clay particles is raised, because hydrophilic surfaces induce lamellar ordering locally. Using small angle neutron scattering, the structure of microemulsions was observed as a function of clay content. The critical concentration is indicated by discontinuous structural changes and depends on the platelet diameter and is explained by the free energy of the platelets competing with the fluctuating medium. The gel phase transition is observed in the spectroscopic measurements where the diffusion motion is widely suppressed in the gel phase, but otherwise superimposes with the membrane undulations.



## 1. Introduction

Microemulsions are thermodynamically stable mixtures of oil and water [1–3] that are mediated by the surfactant. Locally, there are oil and water domains that are observable by scattering experiments [4] that are separated by the surfactant film. The domain sizes are usually a few nanometers and display shapes from spherical droplets over elongated droplets to the bicontinuous sponge

* Corresponding author at: Jülich Centre for Neutron Science at MLZ, Forschungszentrum Jülich GmbH, Lichtenbergstrasse 1, 85747 Garching, Germany.
*E-mail address:* h.frielinghaus@fz-juelich.de (H. Frielinghaus).

https://doi.org/10.1016/j.jcis.2018.04.032
0021-9797/

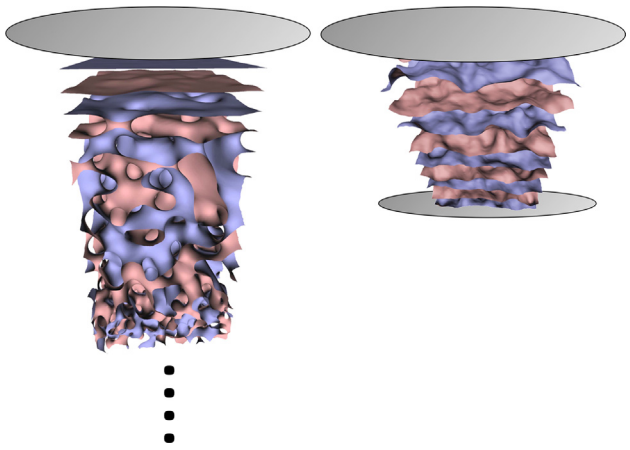

**Fig. 1.** A sketch for the phase transition of capillary condensation of a microemulsion between clay platelets.

phase. Also liquid crystalline order between the domains can be observed. In the following we restrict ourselves to the bicontinuous microemulsion. The explanation for this choice of the system is a relatively simple handling (equilibrium means reproducibility) and very well documented characterization. For instance, a long history is written on bicontinuous microemulsions with polymeric additives [5–9]. In terms of applications, microemulsions are used as cleaning agents [10] and are discussed as fuels with much less pollutant emissions from the combustion [11,12].

When exposing the microemulsion to hydrophilic surfaces, a lamellar order is locally induced next to the interface [13]. From spectroscopic measurements, we know that the membrane fluctuations in microemulsions are faster in the lamellar state [14]. This is connected to the lubrication effect [15], because the lamellae can slide off easier and the motions are faster. In spectroscopic measurements with hydrophilic clay particles, we could show, that the platelet diameter causes a cutoff of the undulation modes, and larger platelets cause a better order with longer wavelength modes [16]. In rheology experiments this microscopic effect was observed macroscopically [17].

So far, all experiments stayed at relatively low clay concentrations, when the system is still liquid [16,17]. The lamellar fraction in microemulsions with 1% clay is around 25% in volume [16]. From the predictions of a capillary condensation [18,19], we were motivated to study higher clay concentrations (see Fig. 1). An interesting detail of the clay structure in microemulsions is the speculation that the particles arrange on a checkerboard structure where the next layer places particles on holes of the original one [17]. When the layer of lamellar surfactant membrane order keeps its extension, at a particular clay platelet distance the whole system must undergo a phase transition to lamellar only. We tried to observe this phase boundary using small angle neutron scattering (SANS) and neutron spin echo (NSE) spectroscopy. The results are discussed in this order.

## 2. Materials

The non-ionic surfactant tetra-ethylene glycol mono-decyl ether ($C_{10}E_4$) was purchased from Bachem Distribution Services, Weil am Rhein. The heavy water ($D_2O$) and perdeuterated n-decane were purchased from Armar Chemicals, Döttingen. All chemicals were used without further purification. The batch microemulsions with film and bulk contrast were mixed with 17 vol% surfactant and 41.5 vol% heavy (normal) water and 41.5 vol % protonated (deuterated) oil, using the densities of 0.974, 1.105 (1.000), 0.840 (0.97) g/cm$^3$, respectively. All microemulsions were stable at a temperature window of 25 °C (27 °C) (±2K) observed by visual inspection of turbidity.

Clay particles were obtained from Süd Chemie (Rockwood), now belonging to the BYK chemicals group. We received two types of clay: Laponite RD (LRD) that is reported to have a diameter of 25–30 nm, and Montmorillonite (MMT) EXM 757 had a diameter of approx. 500 nm. The Laponite material was used without further cleaning. The Montmorillonite material was dispersed in deionized water by sonication over night, centrifuged, and the liquid portion dried using a rotor vap and a vacuum oven. The particles were dispersed in the microemulsion with given volume percentages using the density of 2.6 g/cm$^3$. The dispersions were sonicated from 1 to 3 h. The samples were stable in the same temperature range by showing little turbidity – the particles caused light scattering.

## 3. Experimental

Small angle neutron scattering (SANS) experiments have been performed on KWS-1 [20,21] within the Heinz Maier-Leibnitz Zentrum (MLZ) at the research reactor FRM-2 in Garching/Munich. The neutron velocity selector was set to 5 Å wavelength with a FWHM spread of 10%. The instrument has a length of 20 + 20 m for collimation and detector. The collimation was set to 20 m with an entrance aperture of 3 × 3 cm$^2$. The detector distance was varied between 20 m, 8 m and 1.5 m to cover the full accessible $Q$-range. The scattering vector Q was calculated as the function of the scattering angle θ and the wavelength λ according to $Q = 4\pi \sin(\theta/2)/\lambda$. The macroscopic cross section $d\Sigma/d\Omega(Q)$ was calibrated using a secondary plexiglass standard and transmission. Longer measurements (1 h) of plexiglass served for a pixel-wise sensitivity measurement. All measurements were corrected against the empty cell, the empty beam and dark current background. All samples were heated to 25 °C using a Peltier element against water-cooling to obtain the one-phase microemulsion.

Neutron spin echo (NSE) spectroscopy measurements have been performed on J-NSE [22] within the MLZ at the research reactor FRM-II in Garching, at the SNS-NSE at the Spallation Neutron Source in Oak Ridge [23], and at IN-15[24,25] at the Institut Laue Langevin. The neutron velocity selector was set to 8 Å wavelength. Details of the method and calibration are given in Ref. [26]. The result of the measurement is the intermediate scattering function $S(Q,t)$, given by:

$$S_{\mathrm{coh}}\left(\vec{Q},t\right) = \sum_{m,n}\langle exp\left(i\vec{Q}(\vec{r}_m(t) - \vec{r}_n(0))\right)\rangle \quad (1)$$

with $\vec{r}_m$ the position of surfactant molecule $m$. $S(Q,t)$ is the Fourier transform of the real space van Hove correlation function into reciprocal space. All measurements were calibrated against unwanted background and the instrument resolution.

## 4. Results

The bulk contrast samples at particle concentrations between 0.5 and 2.5 vol% were characterized using SANS (Fig. 2, Supplementary Material: Fig. S1). We see a clear correlation peak at approx. Q = 0.035 Å$^{-1}$ that results from the oil and water domains that alter on a local scale. An upturn towards lower Q < 0.01 Å$^{-1}$ is observed due to the inhomogeneities that the particles cause. The power law is close to the ideal Porod surface scattering $P \times Q^{-4}$. At high Q > 0.2 Å$^{-1}$ the scattering levels off due to the non-corrected incoherent scattering. It allows for crosschecking the absolute calibration. All scattering curves were fitted by a semi-empirical formula:

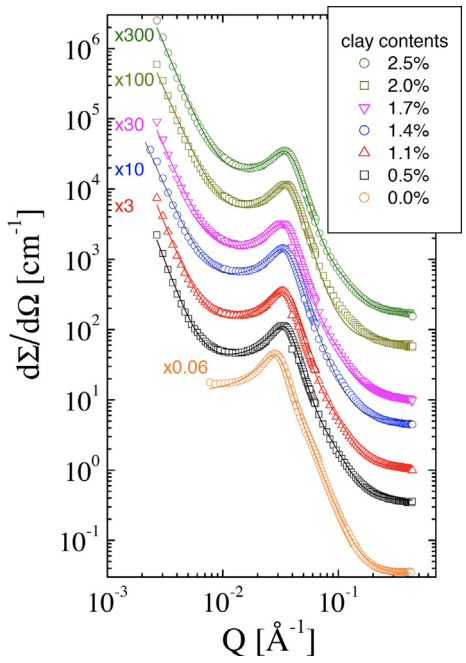


**Fig. 2.** The small angle scattering of microemulsions with dispersed MMT particles. For clarity, the different clay contents are shown with shifted curves according to the numbers given in the left upper corner. Most error bars are similar to the symbol size.

$$\frac{d\Sigma}{d\Omega}(Q) = PQ^{-4} + \left[\frac{A_0}{Q^4 - 2\left(k_0^2 - \xi^{-2}\right)Q^2 + \left(k_0^2 + \xi^{-2}\right)^2} + \frac{A_1 \mathrm{erf}^{12}\left(\frac{1.06QR_g}{\sqrt{6}}\right)}{Q^4 R_g^4}\right] \times \exp\left(-\sigma^2 Q^2\right) + b_{ckgr} \quad (2)$$

with the amplitudes P, $A_0$, $A_1$, and $b_{ckgr}$. The alternating oil and water domains are described with a wavevector $k_0$ and a correlation length $\xi$ that result from the Teubner-Strey formula [27]. This long-wavelength approach does not describe the actual surfaces of the microemulsion locally, and the additional term with the prefactor $A_1$ comes into play [28]. It relates to a domain size $R_g$. All surfactant surfaces show a roughness $\sigma$. Many of these terms have technical quality; thus we only discuss the magnitudes of the correlation length $\xi$ (connected to the peak width), the domain spacing $d = 2\pi/k_0$ (with the approximate peak position $Q_{max} \approx k_0$), and the Porod intensity at $Q = 0.0033$ Å$^{-1}$ (we selected a finite Q within the measured Q-range to avoid an extrapolation with lower accuracy), that are shown in Figs. 3–5. The critical clay content of the capillary condensation is estimated by the trends of all three figures together (1.8% MMT and 1.3% LRD). The characteristic values of the pure microemulsion [6] are added to all figures, but omitted in this discussion.

The correlation length $\xi$ (Fig. 3) shows a clear discontinuity at the critical concentration. For the MMT the correlation length increases at this point, indicating that the degree of order is increased at the phase transition, while $\xi$ decreases for the LRD, indicating the low degree of order for small platelets. The general trend in either phase of the MMT system is a decrease towards higher clay contents, while that the spacing increases (Fig. 4) with a larger fraction of surfactant participating in fluctuations.

The d-spacing *d* (Fig. 4) also shows a discontinuity at the critical concentration. It is very clear for the MMT system. The sudden decrease goes together with the higher degree of order that allows denser membrane packing. In the LRD system this discontinuity is only obvious in concert with the evolution of correlation length and Porod scattering (Figs. 3 and 5).

The Porod scattering (Fig. 5) also indicates the critical clay concentration. While in the MMT system the behavior is discontinuous, the LRD system only shows a kink.

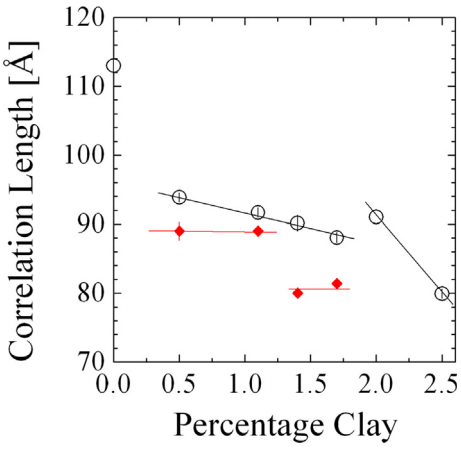


**Fig. 3.** The correlation length of the SANS data as a function of the clay concentration. The open dots correspond to MMT dispersions, and the diamonds to LRD dispersions. The lines are guides for the eye. Most error bars are similar to the symbol size.

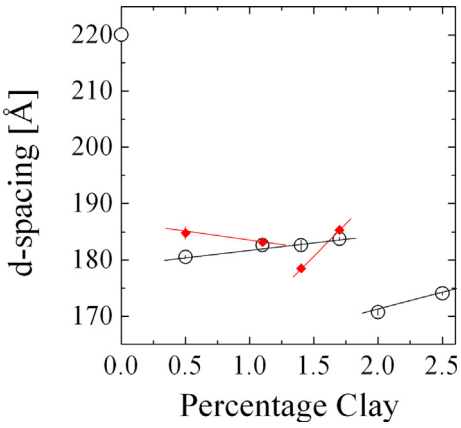


**Fig. 4.** The d-spacing of the SANS data as a function of the clay content. The open dots correspond to MMT dispersions, and the diamonds to LRD dispersions. The lines are guides for the eye. Most error bars are similar to the symbol size.

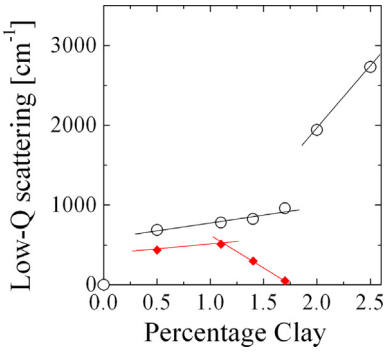


**Fig. 5.** The Porod scattering at $Q = 0.0033$ Å$^{-1}$ as a function of the clay content. The open dots correspond to MMT dispersions, and the diamonds to LRD dispersions. The lines are guides for the eye. Most error bars are similar to the symbol size.

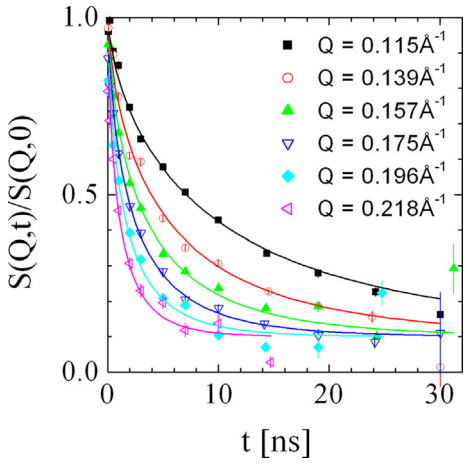


**Fig. 6.** Relaxation curves of the MMT system at 1.5 vol% clay with a film contrast microemulsion. The lines result from a fit of a stretched exponential with an elastic contribution of 0.1 for all Q-values.

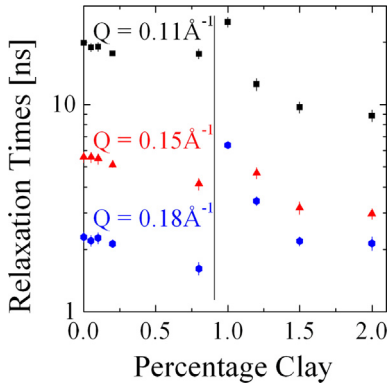


**Fig. 7.** The relaxation times of the MMT system under film contrast with varying clay contents. A clear phase boundary is obtained at 0.9 vol% clay.

NSE data with the MMT clay were taken with the microemulsion being in film contrast. The example of 1.5 vol% clay is depicted in Fig. 6. We can clearly see that there is an elastic contribution of ca. 0.1 for all Q-values resulting from the large clay particles. All curves were described by a stretched exponential [29,30] with an elastic contribution $A$ according to:

$$\frac{S(Q,t)}{S(Q,0)} = A + (1-A)\exp(-(\Gamma t)^{\beta}) \quad (3)$$

The stretch exponent in the large Q-limit takes the value $\beta = 2/3$. The relaxation times $\tau$ are summarized in Fig. 7. For completeness, we added the lower clay contents from Ref. [16]. We can see a clear discontinuity at ca. 0.9% clay content. All relaxation times of 1% clay content are considerably larger than at 0.8%. This phase boundary is not the aforementioned capillary condensation but the gel transition as discussed in the literature [31]. The slowing down at the phase transition is a clear indication.

## 5. Discussion

The strongest criterion for a phase transition is usually the discontinuity of the correlation length as observed for the LRD system. The MMT system displays a much suppressed discontinuity, but together with the discontinuities of the domain spacing and the Porod scattering we can be sure about this point of the phase transition. We specify the critical clay concentration of the MMT and LRD clay to be 1.8% and 1.3%. The difference of the structural characteristics of the phase transition is astonishing though. An attempt of explaining this finding is that the LRD acts against a well-defined lamellar phase, and so the correlation length suddenly decreases at the phase boundary, while MMT promotes the well-defined lamellar structure (the correlation length slightly increases) and the fluctuation spectrum is more suppressed allowing for a denser lamellar phase (with considerably lower d-spacing).

The strongest difference is the tendency of the Porod scattering in the lamellar phase. While in the MMT system the Porod scattering increases dramatically, it nearly vanishes for the LRD system. The MMT system would possibly lead to smaller crystalline regions with stronger grain boundary scattering, while the LRD system might even have facilitated grain alignment and ordering that leads to such large crystallites that they are not observable in the actual Q-window (in Ref. [17] the low-Q scattering of LRD was 10 times lower under shear). This is understandable because the free energy contribution of the clay particles per unit volume would scale with the particle diameter $d^2$ to $d^4$ by the pure analysis of prefactors [32]. A detailed analysis is missing though. The ordering of clay particles for different particle diameters is not to be confused with the controversial known degree of order of the surfactant membranes.

A completely different effect of gelling is observed in the spectroscopic measurements. The Q-scaling in the gel phase obeys the $Q^3$ dependence of membrane fluctuations [29]. In the liquid phase the q-dependence is slightly stronger than expected, which is mainly due to the relaxation time of the data the lowest Q-values. We attribute this to remaining structure factor influences on the relaxation rate when approaching the correlation peak. Only above $Q > 4Q_0$ the pure $Q^3$ dependence can be safely expected.

Diffusive processes have a typical $Q^2$ dependence of the relaxation rate and are a multiplicative contribution to the relaxation function. This diffusive contribution is determined e.g. by the Hellweg group by dynamic light scattering [33] at much smaller Q-values in microemulsion systems due to the size of the particles therein. With this clay system and the clear indication of a gel phase boundary, we see no hint of diffusive contributions in the gel phase. We can safely neglect diffusion and see only the membrane undulations. On the other hand, we see the acceleration of membrane dynamics much stronger after the gel-transition took place at above 1% clay concentration. The relaxation time decreases, especially in the low-Q region where also the accelerated membrane dynamics has been observed with grazing incidence technique. [14]. This effect is significantly more pronounced than in the fluid phase. Long wavelength undulations at the interface to the clay particles dominate the membrane undulation spectrum obviously in this regime [14]. In Ref. [16], the percentage of lamellar phase approaching 1% clay concentration was found to be about 25%. At higher concentrations in the gel we observe now the clear domination of the long wavelength surface undulations. Diffusive motion in the fluid phase might be the reason for smearing out the effect of accelerated membrane dynamics by the clay below the gel transition. At the transition itself, the relaxation time increases significantly until it decays again monotonically with increasing clay concentration in the gel phase. The capillary condensation does not cause a visible change in the relaxation times, because the MMT promotes the lamellar structure already in the non-condensed phase which agrees with a weak change of the correlation length at the phase transition.

## 6. Conclusions

The capillary condensation of microemulsions was observed experimentally between macroscopic surfaces [18] and described for complex fluids theoretically [19]. The thermodynamically stable bicontinuous microemulsion (sponge in a sponge structure [1,2]) can turn into the non-favored, but well ordered lamellar structure induced by the narrowing flat surfaces on sub-micrometer length scales. As precursors, hydrophilic planar surfaces induce a lamellar structure over a limited range of a few domains [13]. Here the dynamics are accelerated [14], and nanoscale clay particles equally induce the local ordering [16]. Now, we have observed the capillary condensation phase boundary of a microemulsion between clay particles of varying concentration. The critical clay content is larger for larger diameters of the particles (1.3 vol% vs. 1.8 vol%). We therefore proved that clay particles orient themselves face-to-face to accommodate the lamellar microemulsion phase although the order is not necessarily perfect over larger distances. While the lamellar order of the microemulsion locally next to the larger flat interface of the clay particles is known to be better [16], the fluctuating medium of the bicontinuous microemulsion has a stronger influence on the large particles. We conclude that the competing entropy of the bicontinuous microemulsion [15] with the free energy of the clay particles [32] causes this effect. In the spectroscopic effects, we see clear hints of the gel phase boundary [31] at 0.9 vol% clay concentration. In the gel state, the domination of the long wavelength undulations [16] at the interface gets very prominent. For the future, a detailed quantitative analysis of all known contributions [15,32] of the free energy would help to understand the competing effects better. While the viscosity modification of the fluid phase using clay particles has been proved to be highly interesting for considerably reduced or extremely high viscosities [17], the viscosity modification deeply in the gel phase remains an interesting question for the future, where considerably lower and higher viscosities are to be expected.

## Acknowledgements

This research at ORNL's Spallation Neutron Source was sponsored by the Scientific User Facilities Division, Office of Basic Energy Sciences, U.S. Department of Energy. We thank Maxim Belushkin for providing 3d-structures of microemulsions using Monte Carlo simulations.

## Appendix A. Supplementary material

Supplementary data associated with this article can be found, in the online version, at https://doi.org/10.1016/j.jcis.2018.04.032.

## References

[1] R. Strey, Coll. Polym. Sci. 272 (1994) 1005–1019.
[2] M.S. Leaver, U. Olsson, H. Wennerström, R. Strey, U. Würz, J. Chem. Soc., Faraday Trans. 91 (1995) 4269–4274.
[3] S. Engelskirchen, N. Elsner, T. Sottmann, R. Strey, J. Coll. Interf. Sci. 312 (2007) 114–121.
[4] L. Magid, P. Butler, K. Payne, R. Strey, J. Appl. Cryst. 21 (1988) 832–834.
[5] H. Endo, M. Mihailescu, M. Monkenbusch, J. Allgaier, G. Gompper, D. Richter, B. Jakobs, T. Sottmann, R. Strey, J. Chem. Phys. 115 (2001) 580–600.
[6] D. Byelov, H. Frielinghaus, O. Holderer, J. Allgaier, D. Richter, Langmuir 20 (2004) 10433–10443.
[7] S. Maccarrone, D.V. Byelov, T. Auth, J. Allgaier, H. Frielinghaus, G. Gompper, D. Richter, J. Phys. Chem. B 117 (2013) 5623–5632.
[8] S. Maccarrone, J. Allgaier, H. Frielinghaus, D. Richter, Langmuir 30 (2014) 1500–1505.
[9] H.F.M. Klemmer, J. Allgaier, H. Frielinghaus, O. Holderer, M. Ohl, Coll. Polym. Sci. 295 (2017) 911–923.
[10] J. Allgaier, H. Frielinghaus, A. Ostermann, T.E. Schrader, A. Wenzik, Neutron News 26 (2015) 33–35.
[11] I. Kayali, K. Qamhieh, U. Olsson, L. Bemert, R. Strey, J. Dispers. Sci. Technol. 33 (2012) 516–520.
[12] I. Kayali, M. Karaein, K. Qamhieh, S. Wadaah, W. Ahmad, U. Olsson, J. Dispers. Sci. Technol. 36 (2015) 10–17.
[13] M. Kerscher, P. Busch, S. Mattauch, H. Frielinghaus, D. Richter, M. Belushkin, G. Gompper, Phys. Rev. E 83 (2011) 030401.
[14] H. Frielinghaus, M. Kerscher, O. Holderer, M. Monkenbusch, D. Richter, Phys. Rev. E 85 (2012) 041408.
[15] N. Gov, A.G. Zilman, S. Safran, Phys. Rev. E 70 (2004) 011104.
[16] F. Lipfert, O. Holderer, H. Frielinghaus, M.-S. Appavou, C. Do, M. Ohl, D. Richter, Nanoscale 7 (2015) 2578.
[17] M. Gvaramia, G. Mangiapia, V. Pipich, M.S. Appavou, G. Gompper, S. Jaksch, O. Holderer, M.D. Rukhadze, H. Frielinghaus, (2018) arXiv:1709.05198.
[18] P. Petrov, U. Olsson, H. Wennerström, Langmuir 13 (1997) 3331–3337.
[19] V. Babin, A. Ciach, M. Tasinkevych, J. Chem. Phys. 114 (2001) 9585–9592.
[20] A.V. Feoktystov, H. Frielinghaus, Z. Di, S. Jaksch, V. Pipich, M.-S. Appavou, E. Babcock, R. Hanslik, R. Engels, G. Kemmerling, H. Kleines, A. Ioffe, D. Richter, T. Brückel, J. Appl. Cryst. 48 (2015) 61–70.
[21] H. Frielinghaus, A. Feoktystov, I. Berts, G. Mangiapia, J. Large-Scale Res. Facil., https://doi.org/10.17815/jlsrf-1-26.
[22] O. Holderer, M. Monkenbusch, R. Schätzler, H. Kleines, W. Westerhausen, D. Richter, Meas. Sci. Technol. 19 (2008) 034022.
[23] M. Ohl, M. Monkenbusch, N. Arend, T. Kozielewski, G. Vehres, C. Tiemann, M. Butzek, H. Soltner, U. Giesen, R. Achten, H. Stelzer, B. Lindenau, A. Budwig, H. Kleines, M. Drochner, P. Kaemmerling, M. Wagener, R. Möller, E.B. Iverson, M. Sharp, D. Richter, Nucl. Instrum. Methods Phys. Res. A 696 (2012) 85–99.
[24] B. Farago, P. Falus, I. Hoffmann, M. Gradzielski, F. Thomas, C. Gomez, Neutron News 26 (2015) 15–17.
[25] P. Schleger, B. Alefeld, J.F. Barthelemy, G. Ehlers, B. Farago, P. Giraud, C. Hayes, A. Kollmar, C. Lartigue, F. Mezei, D. Richter, Physica B 241–243 (1997) 164–165.
[26] D. Richter, M. Monkenbusch, A. Arbe, J. Colmenero, Neutron spin echo in polymer systems, Advances in Polymer Science vol. 174 (2005).
[27] M. Teubner, R. Strey, J. Chem. Phys. 87 (1987) 3195–3200.
[28] C. Frank, H. Frielinghaus, J. Allgaier, H. Prast, Langmuir 23 (2007) 6526–6535.
[29] A. Zilman, R. Granek, Phys. Rev. Lett. 77 (1996) 4788–4791.
[30] A. Zilman, R. Granek, Chem. Phys. 284 (2002) 195–204.
[31] N. Willenbacher, J. Coll. Interf. Sci. 182 (1996) 501–510.
[32] A.G. García, H.H. Wensink, H.N.W. Lekkerkerker, R. Tuinier, (2017) arXiv: 1711.04143v1.
[33] S. Wellert, M. Karg, O. Holderer, A. Richardt, T. Hellweg, PCCP 13 (2011) 3092–3099.